Internal Report
DESY FH1T–90–01
January 1990

Energy Loss Measurements in a Prototype Drift Chamber for the H1-CJC with Various Noble Gas Mixtures

by

R. Vick, E. Schenuit, H. Spitzer

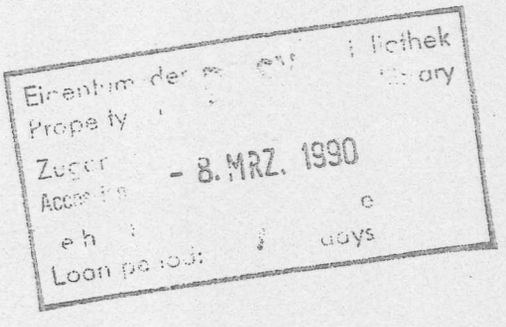

Internal Report
DESY FH1T-90-01
January 1990

Energy Loss Measurements in a Prototype Drift Chamber for the H1-CJC with Various Noble Gas Mixtures

Rainer Vick, Eduard Schenuit, Hartwig Spitzer

II. Institut für Experimentalphysik
Luruper Chaussee 149, D-2000 Hamburg 50

January 21, 1990

Abstract

With a prototype drift chamber for the central jet chamber (CJC) of the H1-experiment energy loss measurements were carried out using three different gas mixtures ($Ar/CO_2/CH_4$, Ar/C_2H_6 and Xe/C_2H_6). Changing beam distance and orientation relative to the signal wires saturation effects in the order of up to 50% have been measured - depending on gas mixture and gas gain. In addition the relative width of the Landau-spectra were measured; they amount to 140%, 100% and 90% respectively.

Introduction

For the H1-experiment at HERA a jet chamber (CJC) is under construction, which will enable the measurement of momentum and energy of particle tracks with $20° \leq \vartheta \leq 160°$ [1]; in addition it will allow particle identification using dE/dx measurements. Various gas mixtures are being considered as counting gases, in particular:

- argon/carbon dioxide/methane (89/10/1)
- argon/ethane (50/50)
- xenon/ethane (50/50)

Before running the CJC at HERA one has to know at which working points the chamber will operate optimally and where one will see systematic disturbances of energy loss measurements. Further it should be investigated, how variations of the electrostatic setup (like changes of the drift field strength) will affect these measurements. The latter is of great importance remembering that the CJC will run in a strong external magnetic field (1.2 T). To review these questions a small drift chamber was developed as a prototype for the H1-CJC with its essential features [2]; extensive tests were carried out with this chamber at DESY in Hamburg ($E_{e^-} \approx 4\ GeV$).

Here we will present the results of energy loss measurements by using three different gas mixtures and two different preamplifiers; particular attention is payed to the question, how far the choice of gas gain and working point of the chamber will enhance the amount of saturation effects and on this way will affect energy loss measurements.

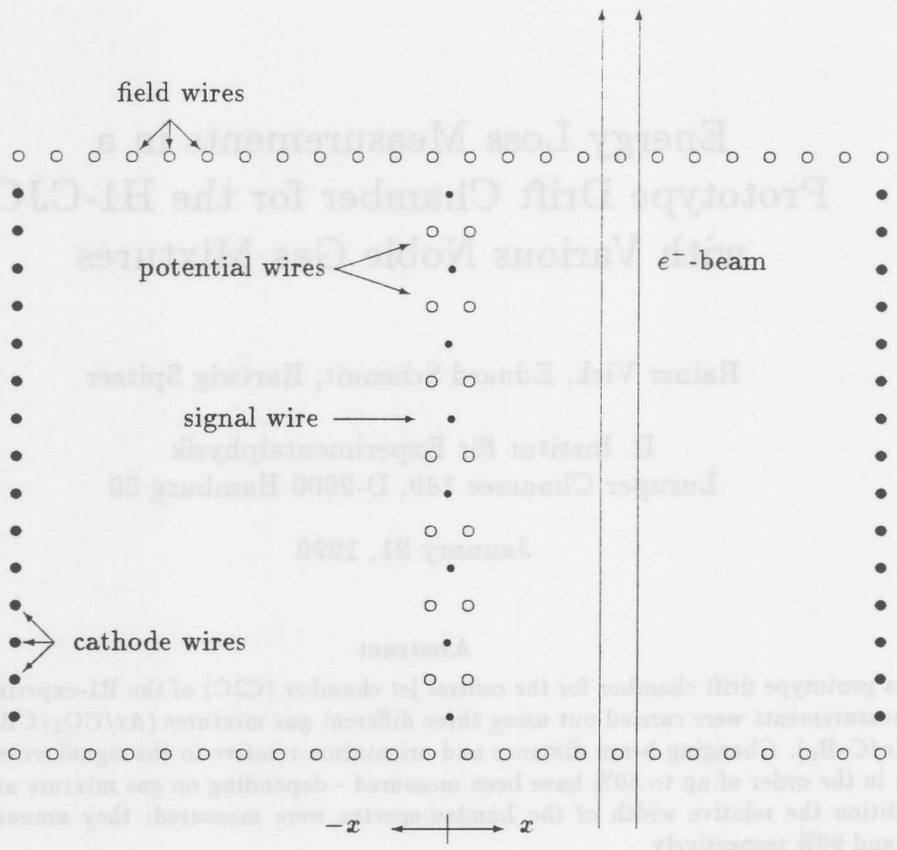

Figure 1: Sketch of the test chamber

Experimental setup

The prototype-chamber (cf. fig. 1) consists of a rectangular super-cell with eight drift cells each of 101.6 *mm* height. In the middle between two of the signal wires (length ca. 1020 *mm*) two potential wires are located in a distance of 5.04 *mm*. Field wires and cathode wires at the edge of the chamber form an almost homogenous drift field of about 48 *mm* width (for more details see [2]).

Each side of a signal wire was read out separately; two different types of preamplifiers, which had been developed for operation at HERA, were at the test disposal:

H1-CJC-low-gain: 10 $mV/\mu A$ amplification,

H1-CJC-high-gain: 100 $mV/\mu A$ amplification.

The amplified signal is sampled by an 8-*bit* FADC-system (type DL 3000) with a frequency of 100 *MHz*. Since the FADC is operated in a nonlinear mode, an effective resolution of 10-*bit* is achieved [4].

The gas gain was adjusted corresponding to the chosen amplifier in such a way that the mean pulse height was 1/20 of the dynamic range (100 mV out of 2000 mV) when electrons crossed the chamber perpendicular to the drift field (i. e. parallel to the signal wire plane). The position of the drift chamber relative to the electron beam was variable; so energy loss measurements were possible in the range of $|x| \leq 40\,mm$ (drift distance) and $25^\circ \leq \vartheta \leq 90^\circ$ (track angle)[1]. The beam

[1] In this paper ϑ represents the angle between signal wire and electron beam orientation.

gas mixture	mixture ratio	E_{drift} $[V/cm]$	v_{drift} $[mm/\mu sec]$
$Ar/CO_2/CH_4$	89/10/1	850	51.4
Ar/C_2H_6	50/50	1000	53.5
Xe/C_2H_6	50/50	1250	42.9

Table 1: List of the analysed gas mixtures with corresponding working points of the chamber (adapted from [3])

was defined by a trigger system which consists of three scintillation counters in coincidence and one additional 'hole'-counter in anticoincidence.

In table 1 the analysed gas mixtures together with the corresponding working points of the chamber are listed (all mixtures ran at standard temperature and pressure); when running the CJC in the solenoidal magnet of H1 the chamber's working point has to be adjusted.

Data analysis

Each triggered event was stored with a data amount of about 4 *kByte*, since each of the 16 FADC-channels recorded the signal during a period of 2.56 μsec. Because of the length of the electron hit (about 200 - 250 *nsec*) only 10% of the whole stored information is of importance for the further analysis. To obtain a fast and effective analysis, at first a reduction of the data to this amount is necessary.

The beginning and the end of a pulse is defined by choosing appropriate thresholds; between these the FADC-counts are picked out. In order to exclude electronic noise and random coincidences with cosmic muons a short track finding routine has been implemented in the preprocessing of the data. This routine exploits the fact, that hits caused by the beam electron have to be recorded by the signal wires almost at the same time, since the beam crosses the chamber parallel to the wire plane all the time (for further information on data reduction and track finding see [5]). After linearization of the FADC-counts the remaining hits are integrated over their full length.

To avoid systematic errors caused by inhomogeneities of the electric field at the edge of the chamber the measurements of the first and the last wire are excluded from further analysis. The pulse integrals of the remaining six sense wires are corrected for variations of the gas gain among them and gain variations of electronic circuits ($\leq 5\%$); in this way one obtains the Landau-spectrum from all signal wires at one beam position, which will enhance the statistical quality of the following interpretations.

Measurement of the mean energy loss and study of saturation effects

The mean energy loss is determined from the so-called 'Truncated Mean', which is a frequently used technique [6]; this method cuts out the high energy tail and uses only a fixed fraction of the lowest energy losses to calculate the mean (in this paper 60% is chosen). When the chamber works properly the mean energy loss should be independent of the drift distance x at a fixed track angle ϑ, because the electrons neither may be amplified nor be absorbed during their drift.

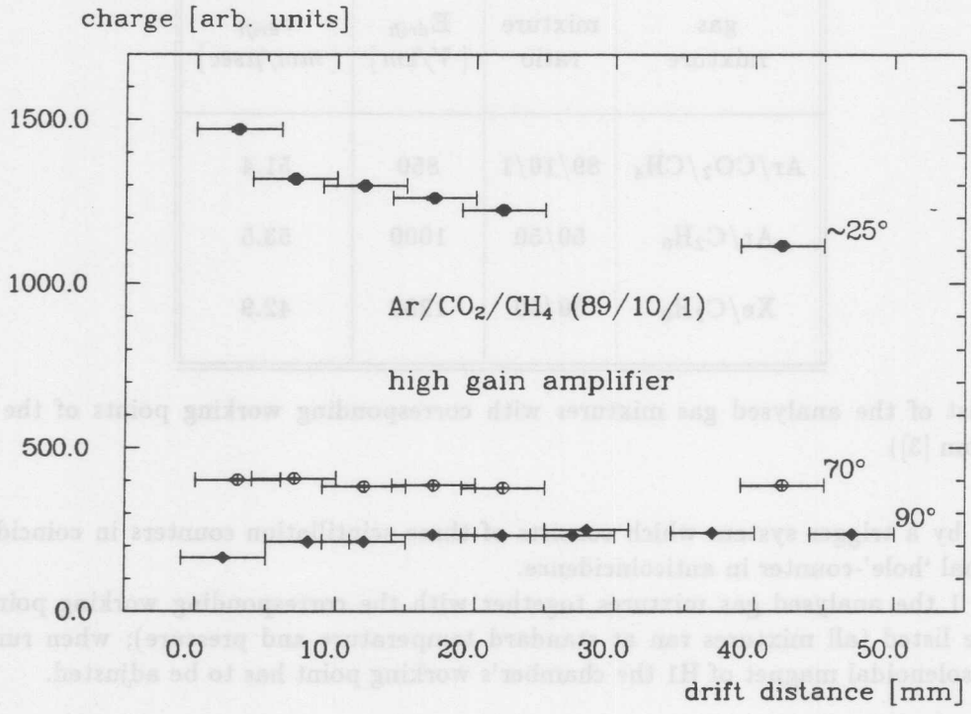

Figure 2: Measured mean energy loss (not corrected for track length) at three different track angles as function of the drift distance using the H1-CJC-high-gain-amplifier

Figure 2 shows the measured mean energy loss versus the drift distance x at three different track angles[2] using $Ar/CO_2/CH_4$. Contrary to the expectations two different trends are clearly visible; a decrease at $\vartheta = 25°$ and an increase at $\vartheta = 90°$, whose effects seem to compensate at about $\vartheta = 70°$.

The decrease of the mean energy loss at $\vartheta = 25°$ is compared for the different gas mixtures in table 2, where the parameter κ from a fit to the function

$$f(x) \propto e^{-\kappa \cdot x}$$

is listed.

A possible reason of this effect could be due to higher contamination by electronegative compounds (like H_2O or O_2), which could lead to an absorption of the drifting electrons[3]. Since the gas was exchanged every two days this decrease is not quite understood.

Compared to the described attachement effects, which at least could be controlled by a gas monitoring and purification system, the consequences of saturation, which are visible in figure 2 at a track angle $\vartheta = 90^c$, are of great importance for the functionality of the chamber. High charge densities close to the signal wire during the phase of gas amplification prevent the detection of all electrons; with increasing drift distance the transverse diffusion of the electrons enables a wider extension of the gas amplification along the signal wire and in this way a smaller charge density. At track angles $\vartheta \leq 90°$ the gas amplification covers a wider region if only because of geometric reasons.

[2]The complete graphic presentation of all results is reserved for the appendix.

[3]Effects with similar amounts have been reported by JADE [8] and OPAL [9]

gas mixture	κ [%/ mm]	$\kappa \cdot v_{drift}$ [%/ μsec]
$Ar/CO_2/CH_4$	0.62	31.9
Ar/C_2H_6	0.50	26.8
Xe/C_2H_6	0.33	14.2

Table 2: Comparison of the attachement factor κ at a track angle $\vartheta = 25°$ and use of the H1-CJC-high-gain-amplifier

Table 3 shows the amounts of saturation effects in different gas mixtures[4] and amplifiers. The saturation is given by the relative decrease of mean energy loss between long and short drift distance

$$\frac{dE/dx_{47mm} - dE/dx_{2mm}}{dE/dx_{47mm}}$$

The use of the H1-CJC-low-gain-amplifier enhances saturation effects due to the higher gas gain.

saturation in % $= \frac{dE/dx_{47mm} - dE/dx_{2mm}}{dE/dx_{47mm}}$		
	H1-CJC-amplifier	
gas mixture	high gain	low gain
Ar/C_2H_6	5.5	43.5
Xe/C_2H_6	14.9	*n.m.*
$Ar/CO_2/CH_4$	29.7	53.1

Table 3: Comparison of saturation effects at a track angle $\vartheta = 90°$ in different gas mixtures

But also if running the chamber with the H1-CJC-high-gain-amplifier a proportionality between energy loss and measured charge is not ensured.

The mean energy loss in $Ar/CO_2/CH_4$ at $|x| = 22\,mm$ - corrected by the geometric factor $\sin\vartheta$ - as a function of the track angle is shown in figure 3. In case of strict proportionality between mean energy loss and measured FADC-pulse integral one would expect a straight line with zero

[4] The mixture Xe/C_2H_6 was measured only with the H1-CJC-high-gain-amplifier.

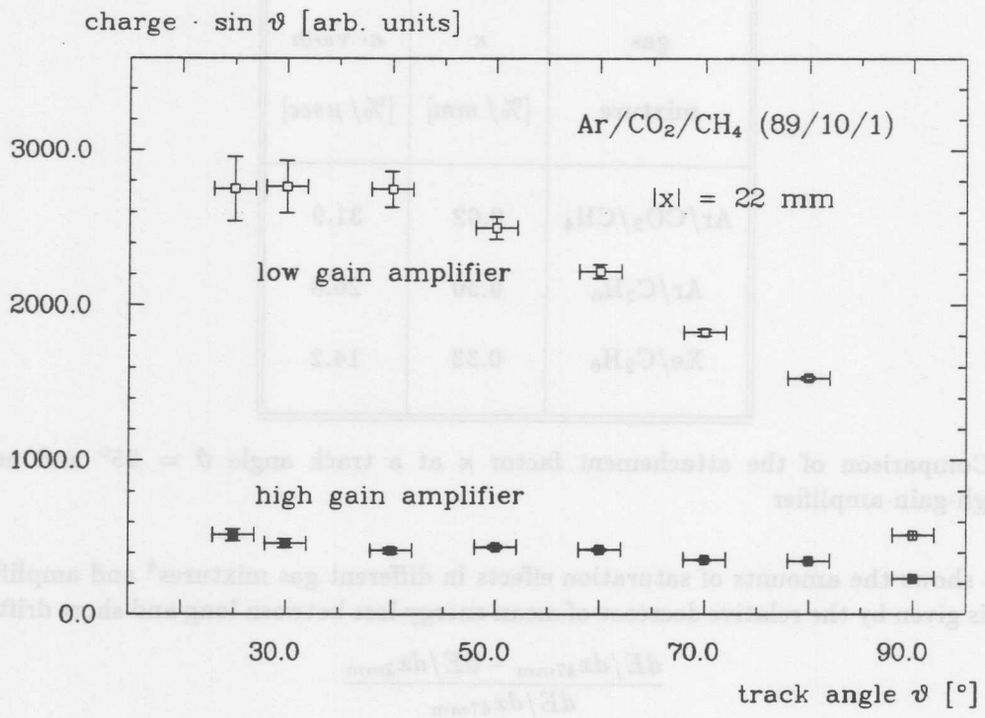

Figure 3: Measured mean energy loss with different gas gain as function of the track angle

slope. Using the H1-CJC-high-gain-amplifier saturation effects seem to vanish sufficiently at a track angle of about 60°. On the other hand the drift chamber together with the H1-CJC-low-gain-amplifier doesn't work in proportional mode at angles above 40° because of the higher gas gain. The measurements revealed similar results for the Ar/C_2H_6 gas mixture. With Xe/C_2H_6 we saw saturation above 50°.

Comparing the mean energy loss at 30° and 80° - as shown in table 4 -, it turns out that

- the use of the H1-CJC-high-gain-amplifier enhances the amount of saturation effects by a factor 2.5,
- if the track is close to the signal wire saturation increases by 25%,
- Ar/C_2H_6 is the most insensitive of the tested gas mixtures.

Variation of the drift field strength

When the H1-CJC will be operated at HERA in the external magnetic field, the drift field strength has to be increased to ensure that the working point of the chamber will stay at the plateau of the drift velocity. Thats why the behaviour of the mean energy loss has been investigated under variation of gas gain and drift field.

Two different gas amplifications - combined with two drift field strengths - were tested with Ar/C_2H_6 for the H1-CJC-high-gain-amplifier. The gas gain was adjusted with the γ-signal of a radioactive ^{55}Fe-source. In figure 4 the mean energy loss is shown as function of the drift distance at $\vartheta = 90^{\circ}$. As one expects the mean energy loss increases by a factor of about two while doubling the gas gain. On the other hand it decreases with rising drift field strength; this is caused by a

saturation in $\% = \frac{dE/dx_{30°} - dE/dx_{80°}}{dE/dx_{30°}}$			
gas mixture	H1-CJC amplifier	drift distance 3 *mm*	drift distance 42 *mm*
Ar/C_2H_6	high-gain	18.1	14.0
$Ar/CO_2/CH_4$	high-gain	28.7	23.3
Xe/C_2H_6	high-gain	33.5	27.3
Ar/C_2H_6	low-gain	50.5	40.9
$Ar/CO_2/CH_4$	low-gain	60.5	42.5

Table 4: Comparison of saturation effects at $\vartheta = 80°$ and $30°$, different amplifiers and drift distance

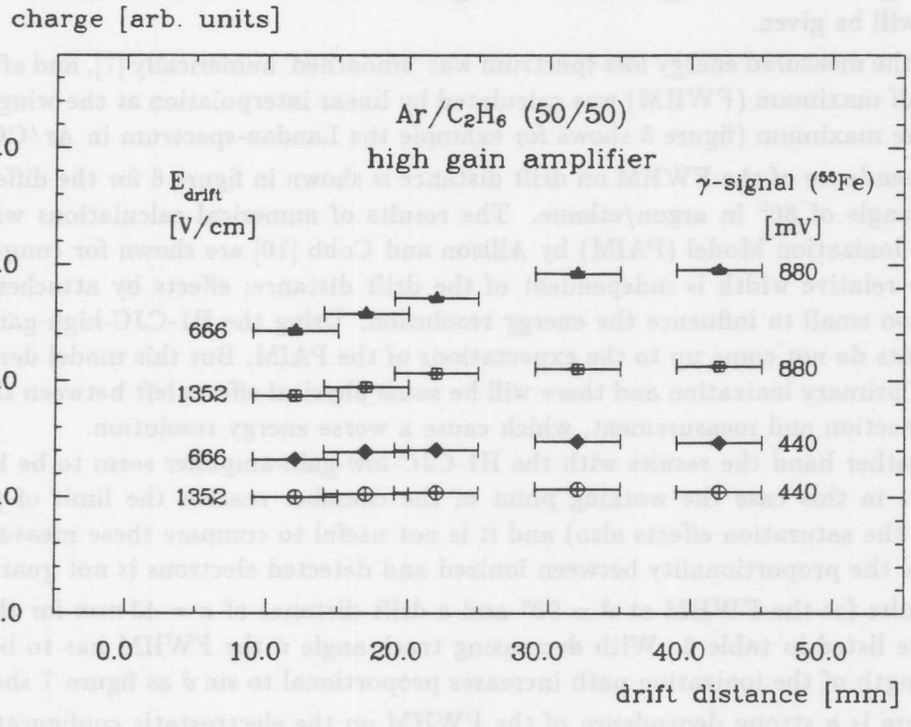

Figure 4: Measured mean energy loss at different drift field strength and gas gain as function of the drift distance

E_{drift} V/cm	^{55}Fe mV	dE/dx $(x = 42\,mm)$	saturation in % $\frac{dE/dx_{42mm} - dE/dx_{2mm}}{dE/dx_{42mm}}$
666	880	1476.5	17.6
1352	880	1063.0	11.9
666	440	733.9	9.6
1352	440	522.6	4.3

Table 5: Comparison of mean energy loss and saturation effects at different gas gain and drift field strength

'strangling' of the drift field lines and in this way by a reduction of the effective ionization track length.

The numerical evaluation (compare table 5) results in a decrease of the mean energy loss down to 72% at double drift field strength in perfect agreement with prior calculations [2]. At the same time as the yield of electrons from the primary ionization diminishes, the amount of saturation effects gets less and less.

Relative width of the Landau-spectra

Because the CJC has to support the feasibility of particle identification in the H1-experiment by measuring the mean energy loss in the region of relativistic rise, finally the achieved energy resolution will be given.

At first the measured energy loss spectrum was 'smoothed' numerically [7], and after that the full width at half maximum (FWHM) was calculated by linear interpolation at the wings and parabola fitting in the maximum (figure 5 shows for example the Landau-spectrum in $Ar/CO_2/CH_4$).

The dependence of the FWHM on drift distance is shown in figure 6 for the different amplifiers at a track angle of 80° in argon/ethane. The results of numerical calculations with the Photon Absorption Ionization Model (PAIM) by Allison and Cobb [10] are shown for comparison. As one expects the relative width is independent of the drift distance; effects by attachement described above are too small to influence the energy resolution. Using the H1-CJC-high-gain-amplifier the measurements do not come up to the expectations of the PAIM. But this model describes only the statistics of primary ionization and there will be some physical effects left between this process and the final detection and measurement, which cause a worse energy resolution.

On the other hand the results with the H1-CJC-low-gain-amplifier seem to be better than the theory. But in this case the working point of the chamber reaches the limit of proportionality (as seen by the saturation effects also) and it is not useful to compare these measurements to the PAIM, since the proportionality between ionized and detected electrons is not guaranteed.

The results for the FWHM at $\vartheta = 90°$ and a drift distance of $x = 42\,mm$ for the different gas mixtures are listed in table 6. With decreasing track angle ϑ the FWHM has to become smaller, since the length of the ionization path increases proportional to $\sin\vartheta$ as figure 7 shows.

Also there is a strong dependence of the FWHM on the electrostatic configuration within the chamber as indicated by table 7. As mentioned above the FWHM decreases with higher gas gain, since the chamber leaves the region of proportional mode.

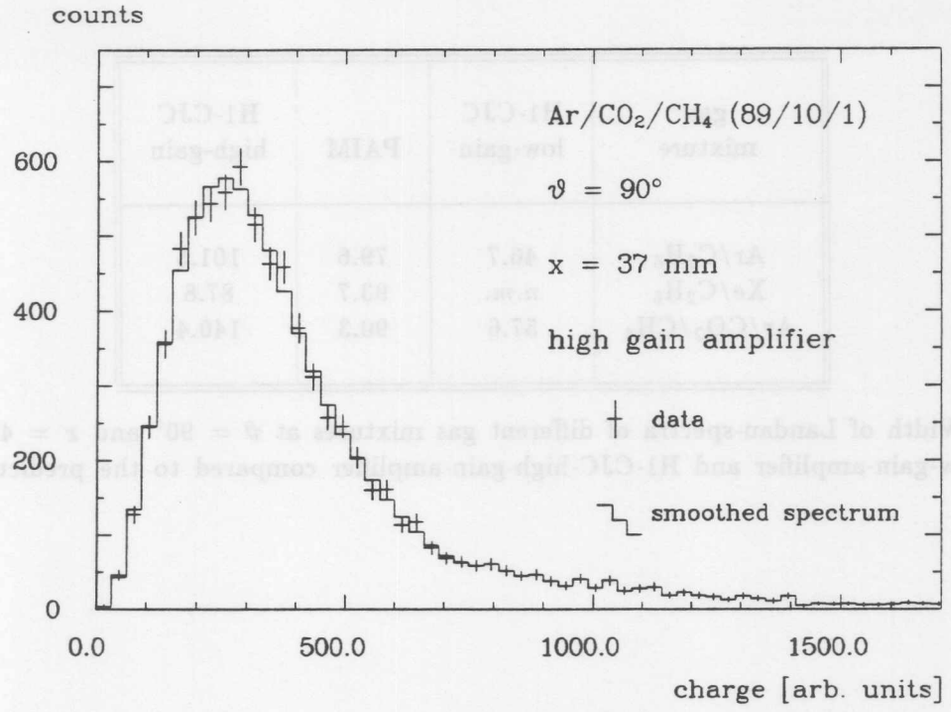

Figure 5: Measured Landau-spectrum in $Ar/CO_2/CH_4$ at $\vartheta = 90°$ and $x = 37\,mm$ using the H1-CJC-high-gain-amplifier

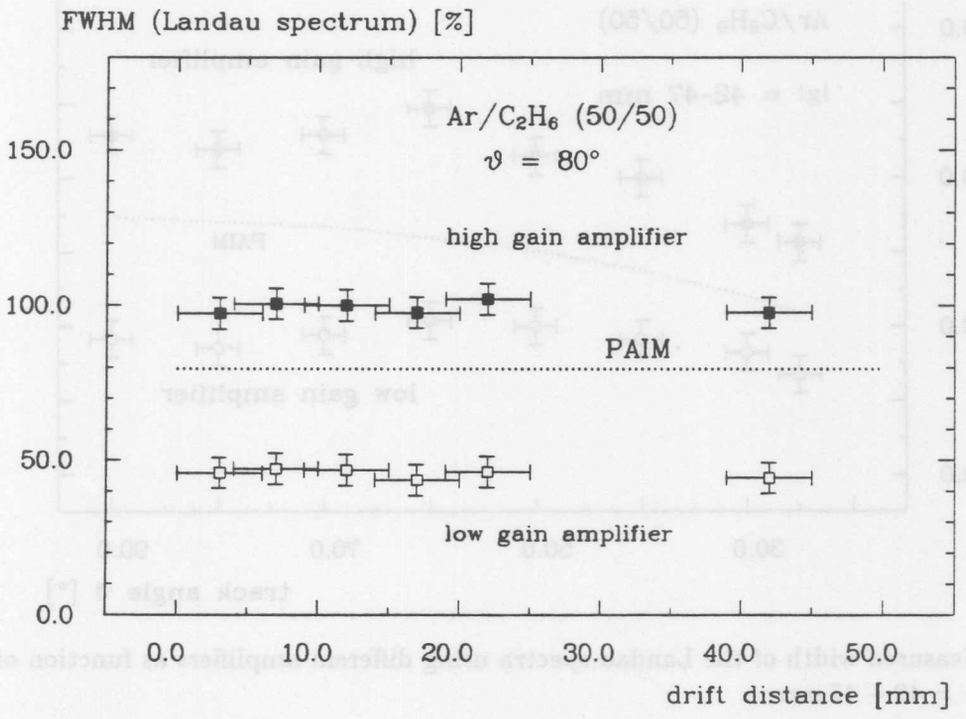

Figure 6: Measured width of the Landau-spectra using different amplifiers as function of the drift distance at $\vartheta = 80°$

gas mixture	H1-CJC low-gain	PAIM	H1-CJC high-gain
Ar/C_2H_6	46.7	79.6	101.5
Xe/C_2H_6	*n.m.*	93.7	87.8
$Ar/CO_2/CH_4$	57.6	90.3	140.4

Table 6: Width of Landau-spectra of different gas mixtures at $\vartheta = 90°$ and $x = 42\,mm$ using H1-CJC-low-gain-amplifier and H1-CJC-high-gain-amplifier compared to the predictions of the PAIM

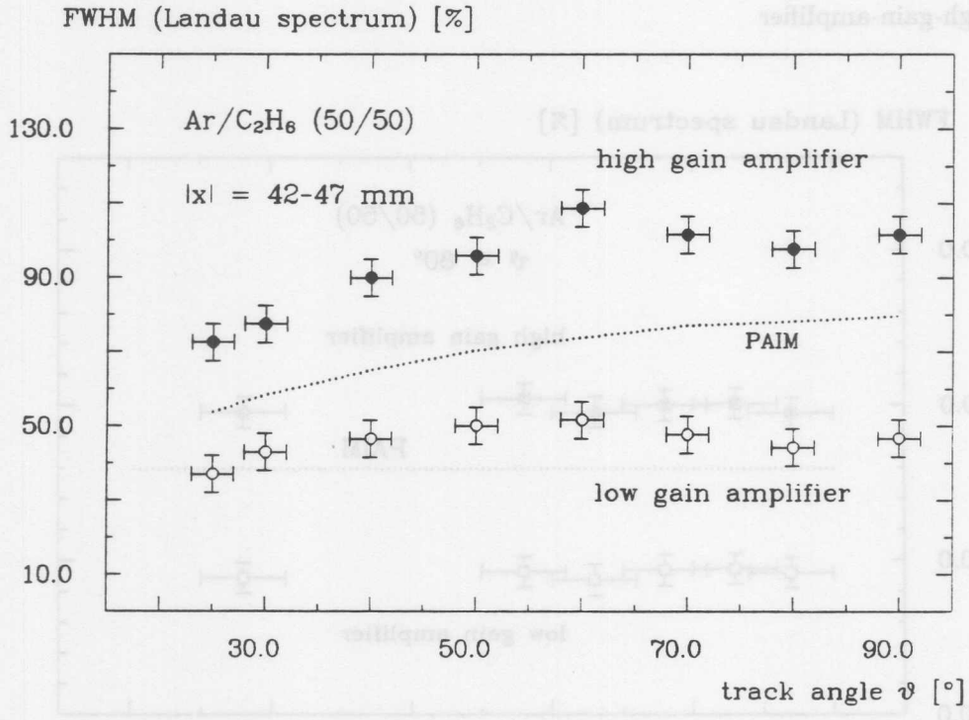

Figure 7: Measured width of the Landau-spectra using different amplifiers as function of the track angle ϑ at $x = 42 - 47\,mm$

E_{drift} V/cm	^{55}Fe mV	FWHM %
666	880	73.8
666	440	79.5
1352	880	88.8
1352	440	109.0

Table 7: Width of the Landau-spectra at different gas gain and drift field strength

With stronger drift field strength the energy resolution becomes worse; this is because of the 'strangling' of drift field lines, which leads to a reduction of the effective ionization path length and in this way to poorer statistics during the ionization process.

Conclusions

The analysis of the experimental results has shown:

- The purity of the gas in the H1-CJC has to be carefully controlled, in order to avoid later additional corrections to the data.
- Using the H1-CJC-low-gain-amplifier strong saturation effects (in the order of up to 50%) will be expected over a wide track angle range ($30° \leq \vartheta \leq 90°$).
- But also if using the H1-CJC-high-gain-amplifier saturation effects cannot be prevented even though with smaller amount (up to 20% for $60° \leq \vartheta \leq 90°$).
- To make use of the energy loss measurements of the H1-CJC for particle identification at the HERA-experiment H1, the operation with the H1-CJC-high-gain-amplifier is recommended, since only this amplifier will ensure the necessary proportional operation mode of the drift chamber.

Acknowledgements are due to J. Groh, K. Johannsen, R. Schmidt and G. Westerkamp for their kind help during the experimental setup and data taking.

References

[1] H1 Collaboration, *Technical Proposal for the H1-Detector*, Hamburg 1986

[2] G. Westerkamp, *Aufbau und Test eines Prototypen für die zentrale Jetkammer des Detektors H1*, Diploma Thesis, Hamburg 1988, DESY F14-88-03

[3] K. Johannsen, *Messungen zur Ortsauflösung an einem Prototypen für die H1-Jetkammer mit unterschiedlichen Gasmischungen und Vorverstärkern*, Diploma Thesis, Hamburg 1989, DESY FH1T-89-05

[4] W. Zimmermann, *Entwicklung des DL3000 FADC Systems (basierend auf dem Heidelberger DL300 System)*, DESY 1986

[5] R. Vick, *Untersuchungen zur e/π-Trennung in der H1-Jetkammer*, Diploma Thesis, Hamburg 1988

[6] W. A. Oran, *Concerning the Use of dE/dx Systems to Measure the Charge and Energy of Relativistic Particles*, Nuclear Instruments and Methods 97 (1971), p. 151;

D. Jeanne et al., *High Energy Particle Identification Using Multilayer Proportional Counter*, Nuclear Instruments and Methods 111 (1973), p. 287;

J. H. Cobb et al., *The Ionization Loss of Relativistic Charged Particles in Thin Gas Samples and its Use for Particle Identification*, Nuclear Instruments and Methods 133 (1976), p. 315

[7] V. Blobel, *SPFT - Smoothing of Noisy Data*, DESYLIB, 1985

[8] K. Ambrus, *Suche nach abnormal ionisierenden Teilchen bei JADE*, Thesis, Heidelberg 1986

[9] H. Breuker et al., *Particle identification with the OPAL jet chamber in the region of the relativistic rise*, CERN-EP/87-97

[10] W. W. M. Allison and J. H. Cobb, *Relativistic Charged Particle Identification by Energy Loss*, Ann. Rev. Nucl. Part. Sci., Vol. 30 (1980), p. 253

Appendix

On the next eight pages the complete graphic presentation of the experimental results is given according to the following list:

Argon/Ethane (50/50)

- Mean energy loss as function of the drift distance using the
  - H1-CJC-low-gain-amplifier 14
  - H1-CJC-high-gain-amplifier 14
- Mean energy loss as function of the track angle ϑ
  - near the sense wire 15
  - far from the sense wire 15
- Relative width of the Landau-spectra (FWHM) as function of ϑ
  - at a mean drift distance 16
  - near the sense wire 16

Xenon/Ethane (50/50)

- Mean energy loss as function of the drift distance using the H1-CJC-low-gain-amplifier . 17
- Relative width of the Landau-spectra (FWHM) as function of ϑ at a mean drift distance 17
- Mean energy loss as function of the track angle ϑ
  - near the sense wire 18
  - far from the sense wire 18

Argon/Carbon dioxide/Methane (89/10/1)

- Mean energy loss as function of the drift distance using the
  - H1-CJC-low-gain-amplifier 19
  - H1-CJC-high-gain-amplifier 19
- Mean energy loss as function of the track angle ϑ
  - near the sense wire 20
  - far from the sense wire 20
- Relative width of the Landau-spectra (FWHM) as function of ϑ
  - at a mean drift distance 21
  - near the sense wire 21

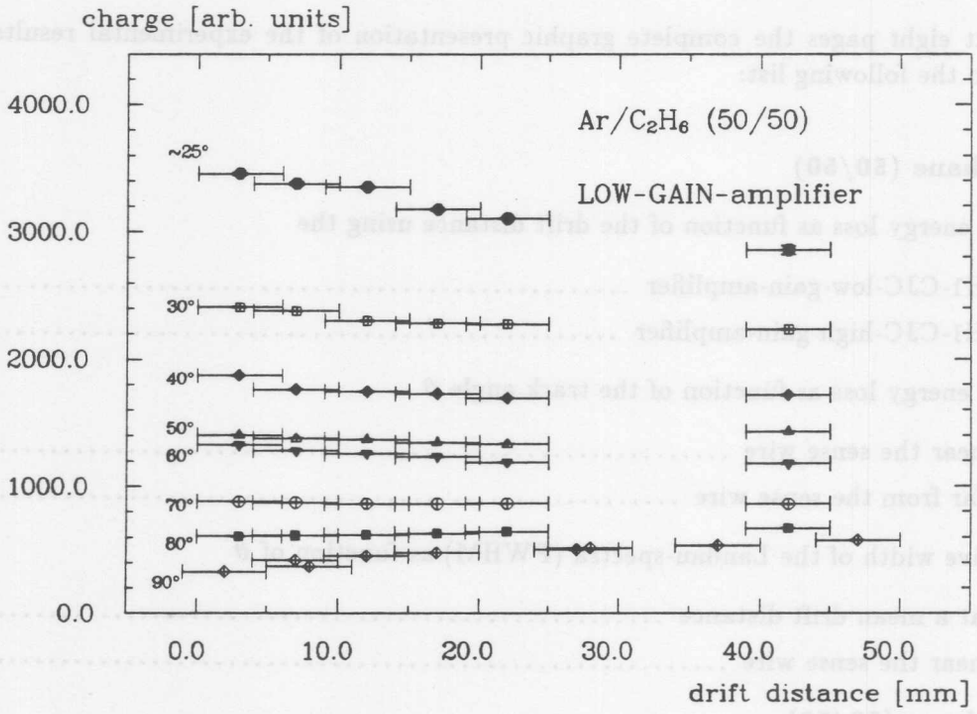

Figure 8: Mean energy loss as function of the drift distance in argon/ethane using the H1-CJC-low-gain-amplifier

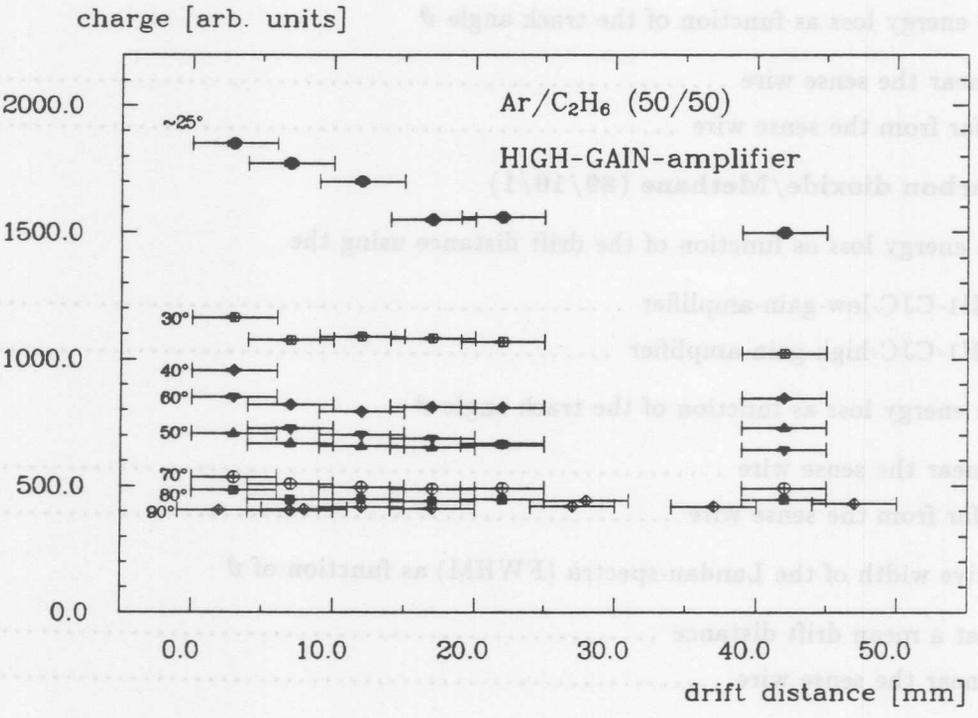

Figure 9: Mean energy loss as function of the drift distance in argon/ethane using the H1-CJC-high-gain-amplifier

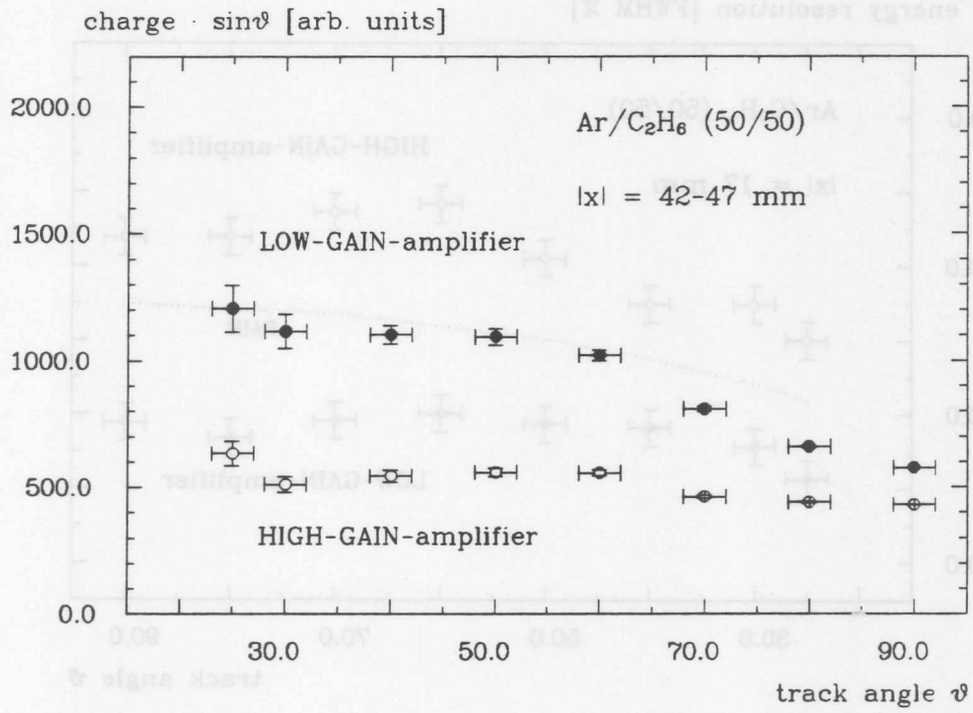

Figure 10: Mean energy loss in argon/ethane as function of the track angle ϑ far from the sense wire

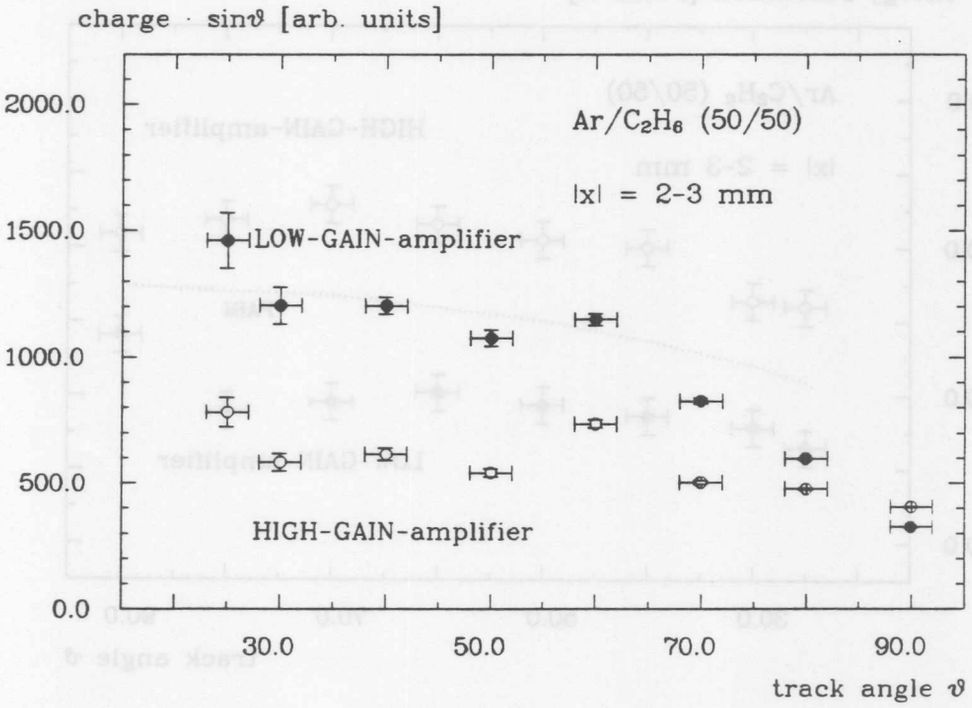

Figure 11: Mean energy loss in argon/ethane as function of the track angle ϑ near the sense wire

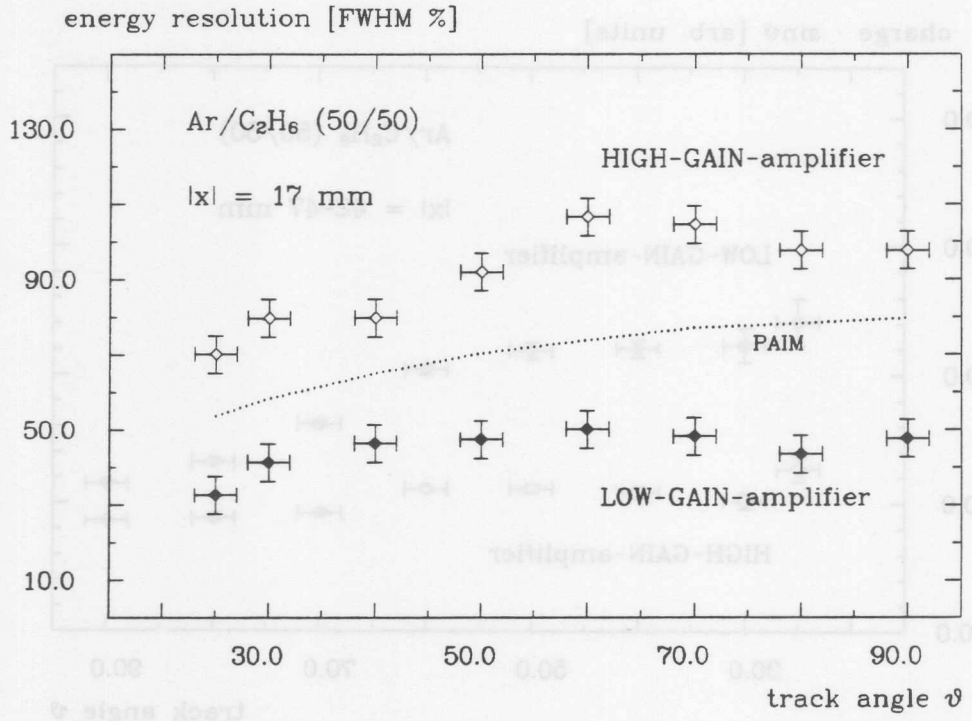

Figure 12: Relative width of the Landau-spectrum as function of the track angle ϑ at a mean drift distance compared to the predictions of the PAIM in argon/ethane

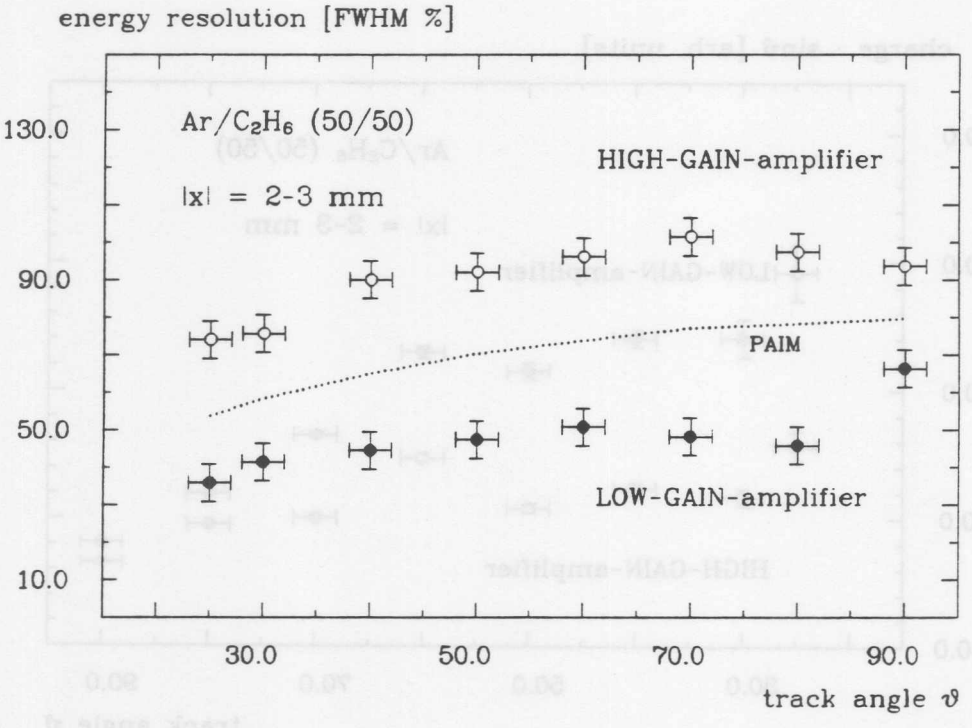

Figure 13: Relative width of the Landau-spectrum as function of the track angle ϑ near the sense wire compared to the predictions of the PAIM in argon/ethane

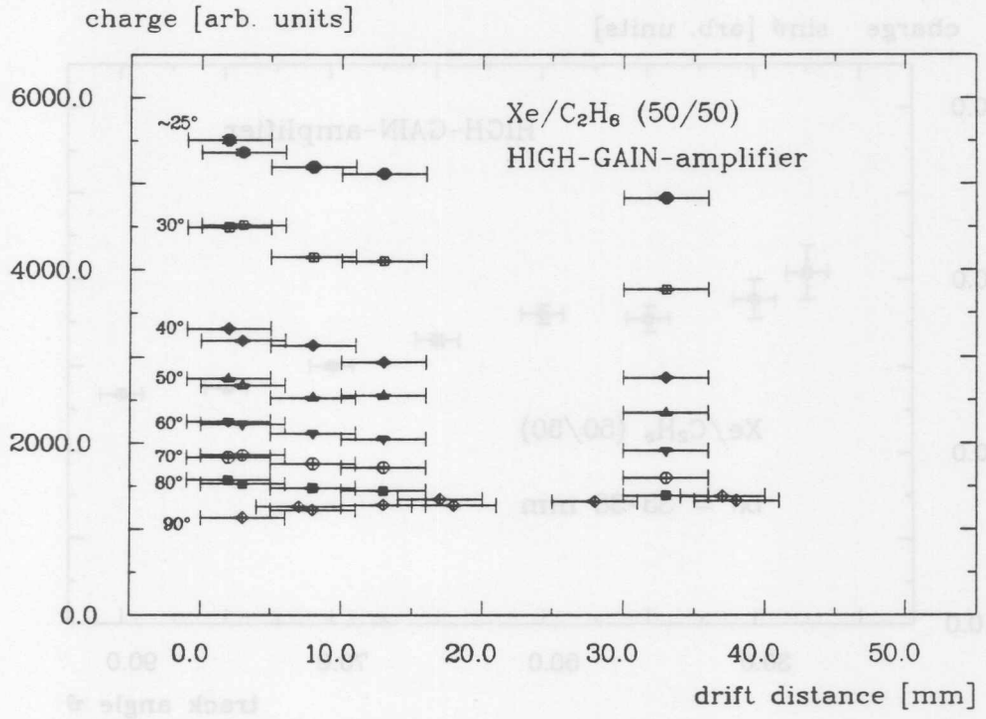

Figure 14: Mean energy loss as function of the drift distance in xenon/ethane using the H1-CJC-high-gain-amplifier

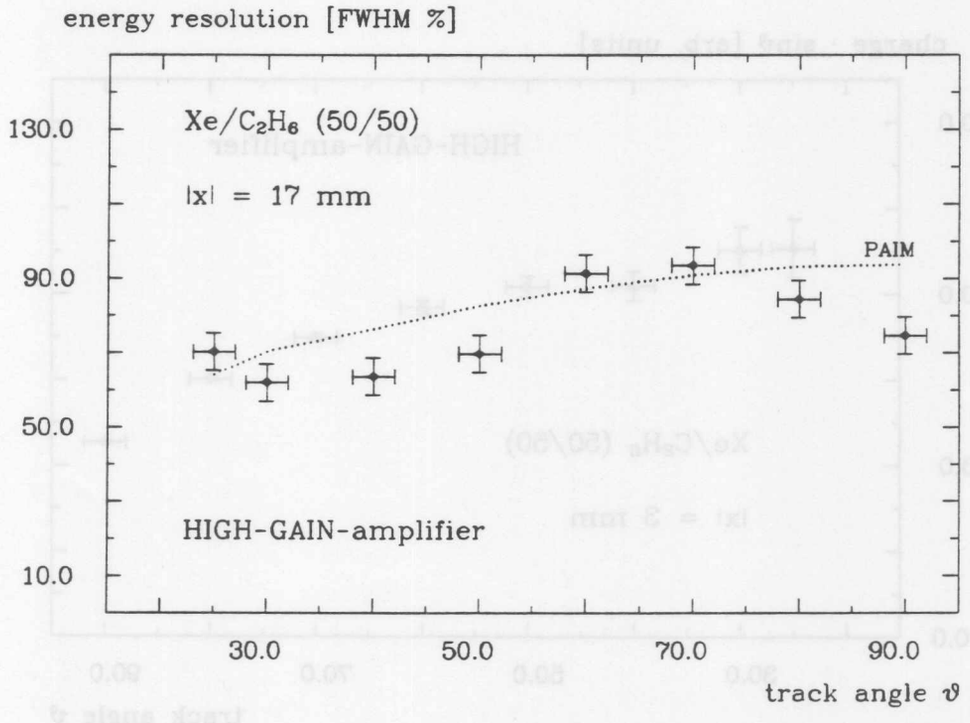

Figure 15: Relative width of the Landau-spectrum as function of the track angle ϑ at a mean drift distance compared to the predictions of the PAIM in xenon/ethane

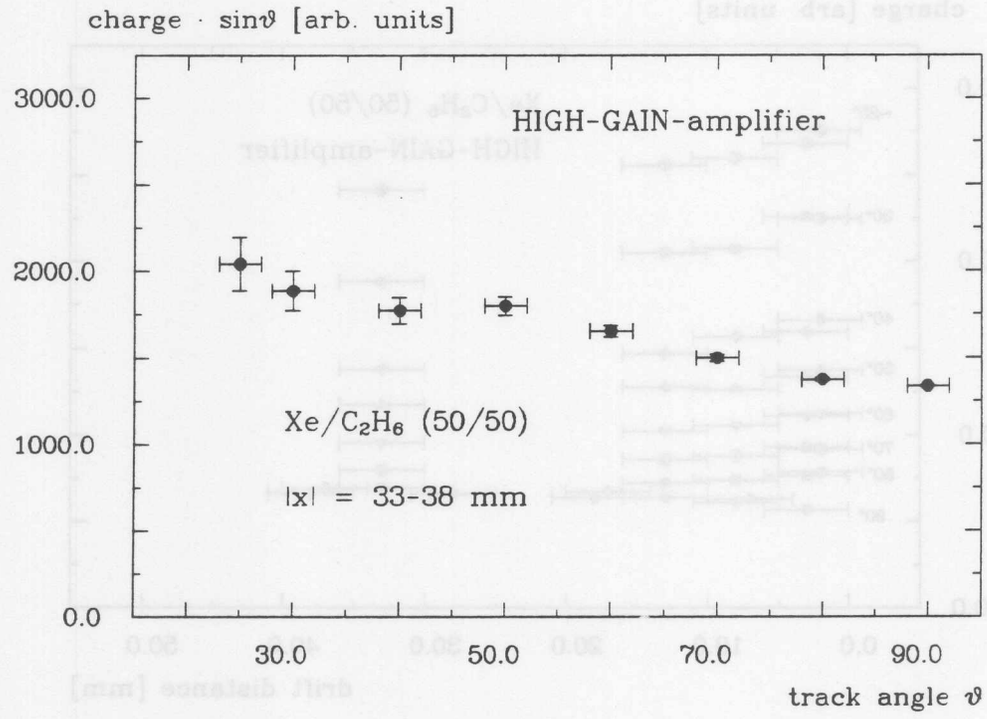

Figure 16: Mean energy loss in xenon/ethane as function of the track angle ϑ far from the sense wire

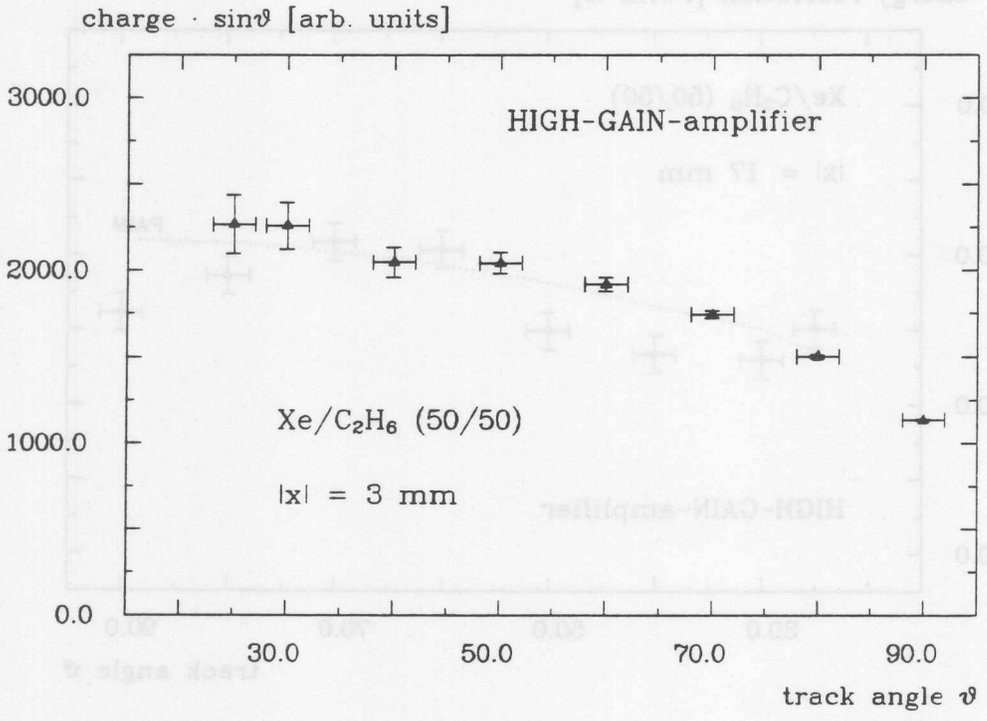

Figure 17: Mean energy loss in xenon/ethane as function of the track angle ϑ near the sense wire

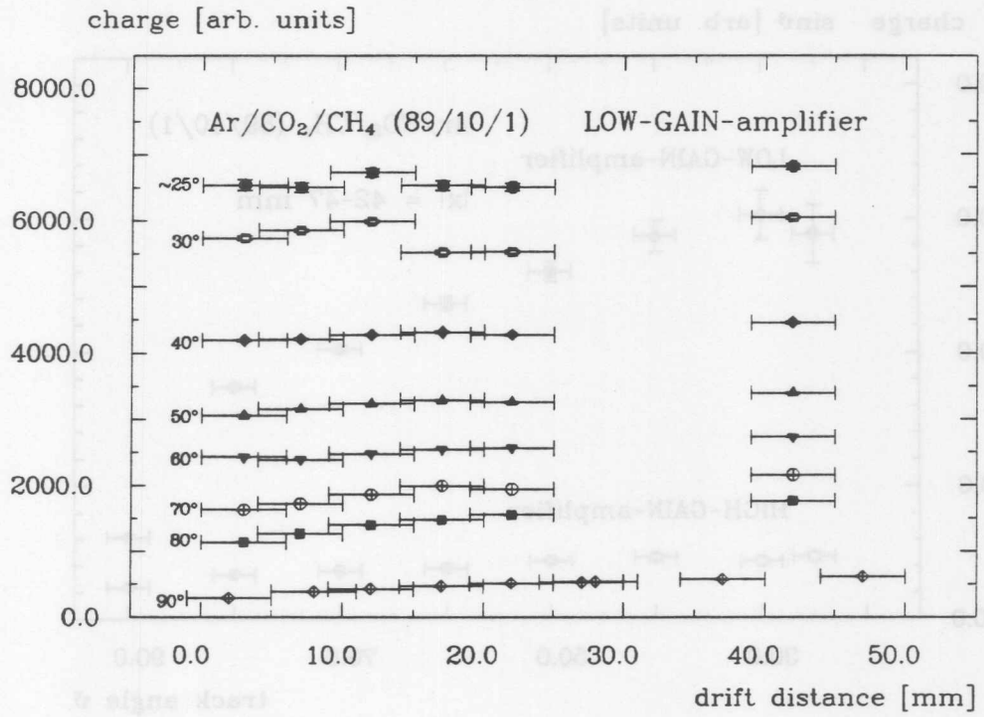

Figure 18: Mean energy loss as function of the drift distance in argon/carbon dioxide/methane using the H1-CJC-low-gain-amplifier

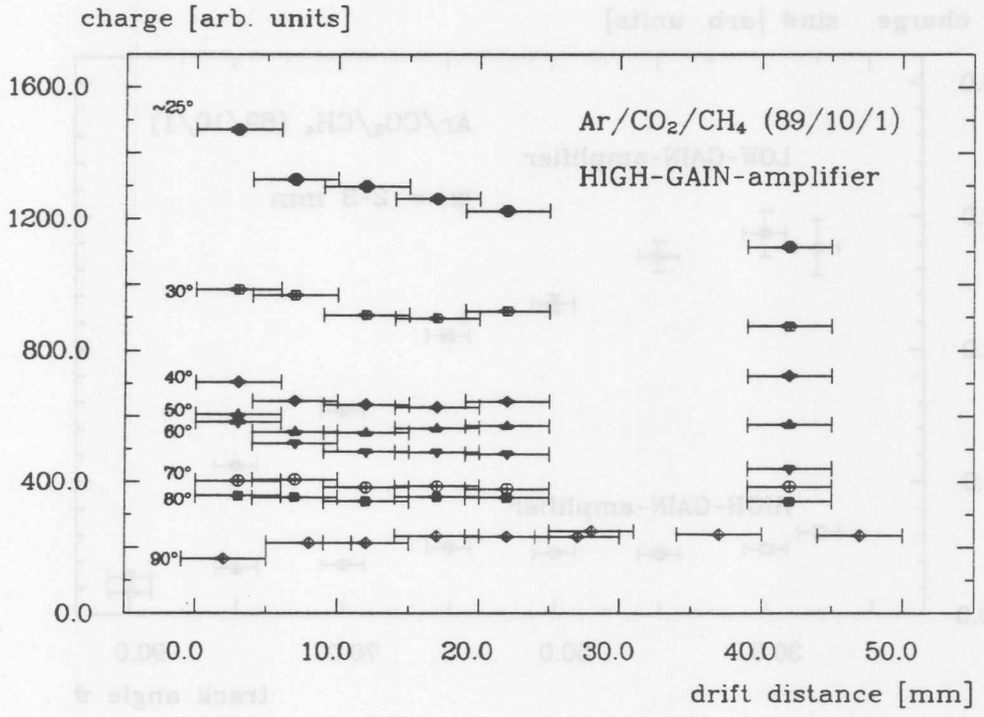

Figure 19: Mean energy loss as function of the drift distance in argon/carbon dioxide/methane using the H1-CJC-high-gain-amplifier

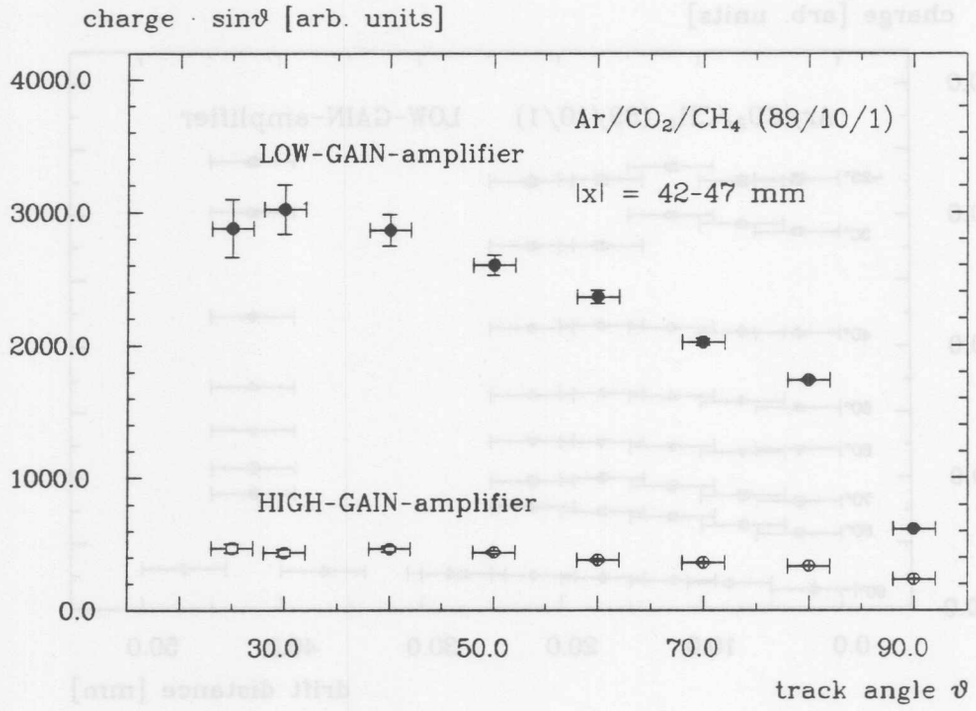

Figure 20: Mean energy loss in argon/carbon dioxide/methane as function of the track angle ϑ far from the sense wire

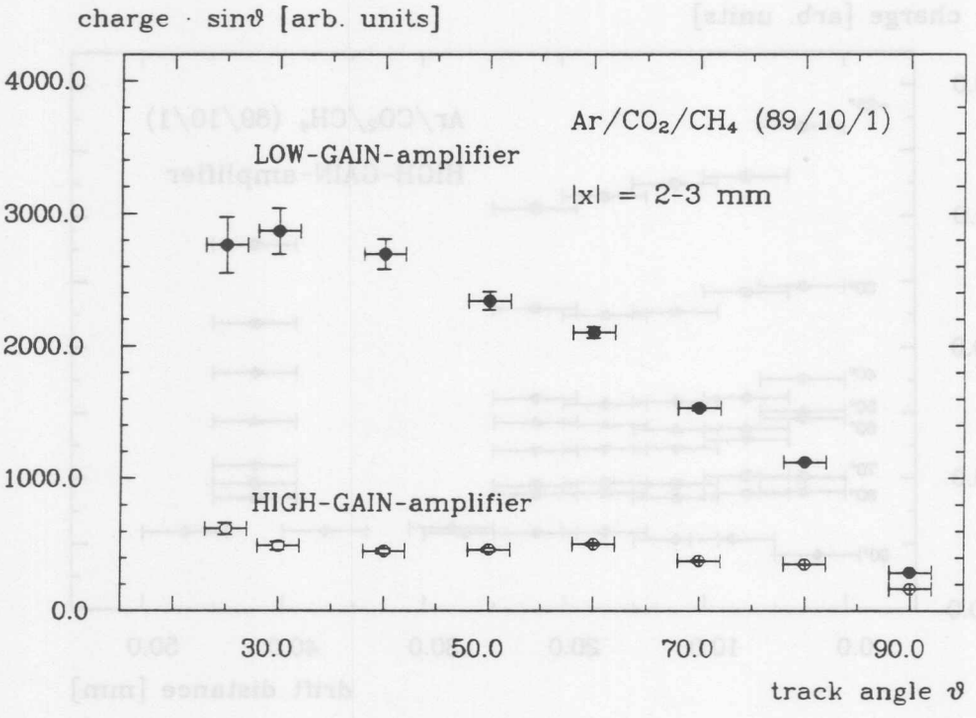

Figure 21: Mean energy loss in argon/carbon dioxide/methane as function of the track angle ϑ near the sense wire

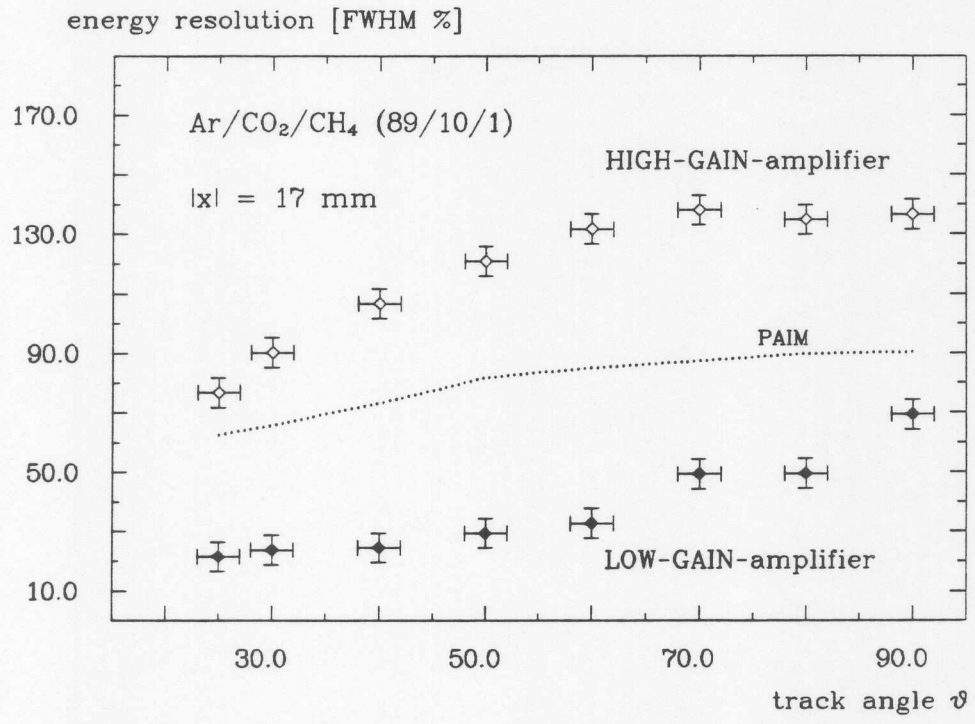

Figure 22: Relative width of the Landau-spectrum as function of the track angle ϑ at a mean drift distance compared to the predictions of the PAIM in argon/carbon dioxide/methane

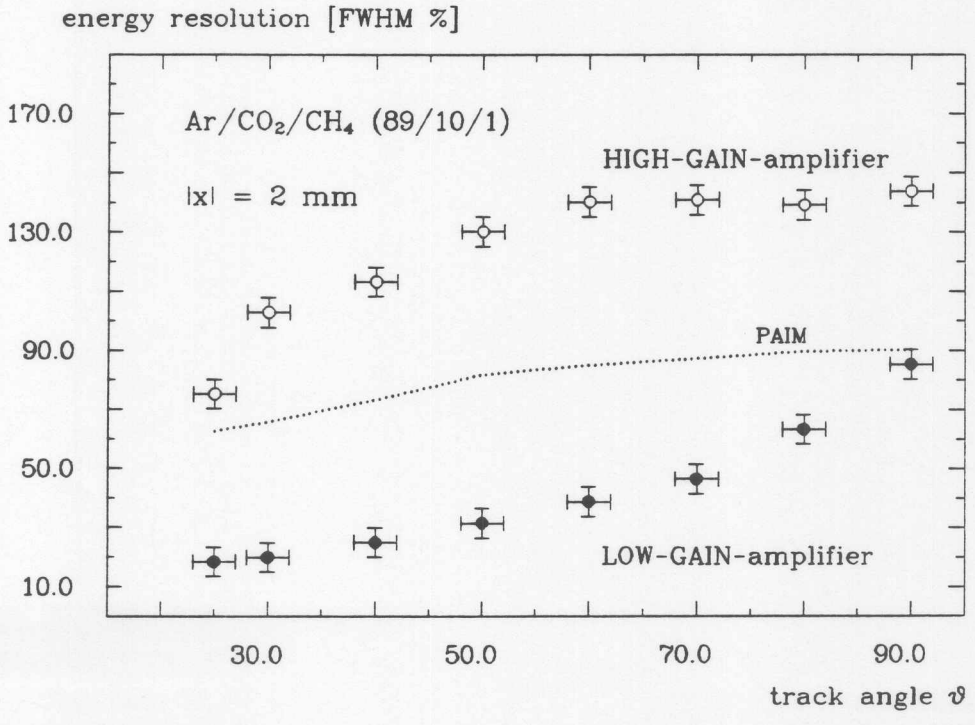

Figure 23: Relative width of the Landau-spectrum as function of the track angle ϑ near the sense wire compared to the predictions of the PAIM in argon/carbon dioxide/methane

Figure 22: Relative width of the Landau-spectrum as function of the track angle ϕ at a mean drift distance compared to the predictions of the PAIM in argon/carbon dioxide/methane

Figure 23: Relative width of the Landau-spectrum as function of the track angle ϕ near the wire compared to the predictions of the PAIM in argon/carbon dioxide/methane